

**Re-engineering Poly (Acrylic Acid) Binder toward Optimized Electrochemical
Performance for Silicon Lithium-ion Batteries: Branching Architecture
Leads to Balanced Properties of Polymeric Binders**

Sisi Jiang¹, Bin Hu¹, Zhangxing Shi¹, Wei Chen^{3,4}, Zhengcheng Zhang^{1,2} and Lu Zhang^{1,2*}

¹Chemical Sciences and Engineering Division, Argonne National Laboratory, 9700 South Cass
Avenue, Argonne, IL 60439, United States

²Joint Center for Energy Storage Research, 9700 South Cass Avenue, Argonne, IL 60439, United
States

³Institute for Molecular Engineering and Materials Science Division, Argonne National
Laboratory, 9700 South Cass Avenue, Argonne, IL 60439, United States

⁴Institute for Molecular Engineering, The University of Chicago, 5640 South Ellis Avenue,
Chicago, Illinois 60637, United States

*Corresponding Author email: luzhang@anl.gov

Abstract

Silicon has been recognized increasingly as a promising anode material for lithium-ion batteries due to its superior (albeit theoretical) capacity. However, the drastic volume changes during lithiation/delithiation cycles hinder the cycling performance, which occur as a result of particle pulverization, loss of conductivity, and an unstable electrode-electrolyte interface. In this report, a series of synthetic polymeric binders, poly(acrylic acid-*co*-tetra(ethylene glycol) diacrylate) — featuring a poly (acrylic acid) (PAA) backbone branched via a short chain of tetra(ethylene glycol) diacrylate (TEGDA) — are developed that edge toward evidencing well-balanced properties to confront capacity fading in Si-based electrodes. The incorporation of ether chain not only leads to the branching architecture of the PAA backbone, thus affecting its mechanical properties, but the ether chain also promotes the conductivity of Li ions. As a result, a synergistic performance improvement was observed in both half and full silicon lithium-ion cells. The best-performing cell using a branched PAA binder (**bPAA**) with a feeding molar ratio ([TEGDA]:[AA]) of 0.2 evidences a 10% increase in initial capacity and a 31% increase in capacity retention over 100 cycles compared to the linear PAA cell. The cross-sectional microscopic images of the cycled electrodes reveal that **bPAA** binders can drastically reduce the electrode expansion. We believe this improvement results from the well-balanced properties of the polymer design, which could be guiding further development for more advanced binder materials.

Introduction

Finding high-energy anode materials suitable for lithium-ion batteries (LIBs) is a crucial pursuit due to the huge demand for high-energy batteries for consumer electronics and electric vehicles.¹⁻³ Silicon (Si), which can form an alloy with lithium (Li), stands out as one of the most

promising anode materials because of its high theoretical specific capacity (3570 mAh/g when alloyed into $\text{Li}_{4.4}\text{Si}$), earth abundance, and mature processing techniques.⁴⁻⁵ However, Si nanoparticles (SiNPs) experience drastic volume changes (up to 300%) during the lithiation/delithiation process, which results in particle pulverization, electrode delamination, unstable electrode/electrolyte interface, and eventually drastic capacity fade.⁶⁻⁷ As a component that works directly with active particles, a binder plays the critical role in affecting the electrochemical performance of Si-based electrodes as it not only holds the integrity of the electrode matrix but also affects the ion conductivity.⁸⁻¹⁰ The widely used binder in graphite-based anodes, polyvinylidene fluoride (PVDF), is not compatible with alloy-type electrodes like silicon as it cannot either accommodate drastic volume changes or provide robust binding strength.¹¹⁻¹² Finding a compatible binder that could enable silicon anode materials has been a very active research topic, and many new binders have been reported. Based on previous reports, polymers with flexible backbones and incorporated polar groups have attracted a lot of attention and have demonstrated improved cycling performance for silicon anodes. Among them, sodium carboxymethyl cellulose (CMC),¹¹ alginate,¹³ and poly(acrylic acid) (PAA)¹² are some representative examples¹⁴. It is believed that these polar groups, like carboxylates, may form chemical bonding with silanol (Si-OH) groups on the surface of SiNPs, thus leading to strong adhesion and less electrode delamination.¹⁵⁻¹⁶ However, simply enhancing one property does not seem to be enough to counteract the rapid capacity fade that may result from a combination of the aforementioned unfavorable issues.

Many properties are desired when it comes to an ideal binder material. Besides adhesion, mechanical properties are also crucial to accommodating drastic volume change or preserving the integrity of electrode structure. Bao *et al.* reported a self-healing polymeric binder by introducing

hydrogen bonds, affording superior viscoelasticity and stretchability.¹⁷ Choi *et al.* incorporated polyrotaxanes into linear PAA as a “pulley” additive to enhance the binder elasticity.¹⁸ Physical or chemical cross-linking is another effective way to tune the mechanical properties of binders given that a three-dimensional (3-D) network is more mechanically sturdy compared to a linear framework.¹⁹⁻²² Other binder properties such as ionic and electronic conductivity,²³⁻²⁴ electrochemical stability, and stiffness also play important roles in affecting the cycling performance.

In addition to the direct impact on cycling performance, making SiNPs into high-quality laminations also largely depends on the binders. The rheological properties of the binder solutions and the slurries are often the dictating factors for a stable slurry sample, which could lead to huge variations in lamination quality. For instance, despite the adverse impact on cycling performance, pre-lithiation to PAA binders only has become a common practice to improve the viscosity and shear-thinning effect of the slurries that may benefit the lamination process.²⁵

It is a challenge to design novel binder materials to accommodate all of these desirable properties, one that requires insightful understanding of the polymer’s structure property, as well as of the binder’s property and cell-cycling performance relationships. Developing multifunctional polymeric binders that can contribute well-balanced properties may be an effective approach to tackling the complicated issues and essentially improving the overall performance of Si-based electrodes.

In this work, we re-engineered the most commonly used binder, linear PAA, by incorporation of a branching ether chain into the backbone via the method of reversible addition–fragmentation chain-transfer (RAFT) polymerization. The introduced ether chains not only change the architecture of the PAA backbone, but also promote the conductivity of the binder materials.²⁶ As

a result, a synergistic improvement in cell performance has been observed in both half cells and full cells containing silicon anodes fabricated by these novel binders.

Experimental Section

Materials

The following materials were purchased from the identified chemicals vendors. 2,2'-Azobis(2-methylpropionitrile) (AIBN, 98%) and RAFT chain transfer agent (CTA) 2-cyano-2-propyl benzodithioate (CPDB, 97%) were purchased from Sigma-Aldrich. Acrylic acid (anhydrous, contains 200 ppm hydroquinone monomethyl ether [MEHQ] as inhibitor, 99%) and tetra(ethylene glycol) diacrylate (TEGDA, technical grade, contains 150–200 ppm MEHQ as inhibitor) were also purchased from Sigma-Aldrich. The inhibitors were removed by passing the reagents through a basic aluminum oxide chromatography column. *N,N*-Dimethylformamide (DMF, American Chemical Society [ACS] grade) was purchased from VWR. Silicon nanoparticles (70–130 nm) were purchased from Nanostructured & Amorphous Materials, Inc. (NanoAmor). MagE graphite flakes (2–4 μm) were obtained from Hitachi, and conductive carbon particles (C45, 50–60 nm) were purchased from Timcal. NCM 523 positive electrodes, which contain 90 wt% $\text{Li}_{1.03}(\text{Ni}_{0.5}\text{Co}_{0.2}\text{Mn}_{0.3})_{0.97}\text{O}_2$, 5 wt% C45, and 5 wt% PVDF binder with a loading of 12.21 mg/cm^2 , were produced by the Cell Analysis, Modeling, and Prototyping (CAMP) facility of Argonne National Laboratory (Argonne). A Gen 2 electrolyte (1.2 M LiPF_6 in ethylene carbonate and ethyl methyl carbonate with weight ratio 3:7) was provided by Tomiyama Pure Chemical Industries. Fluoroethylene carbonate (FEC), used as a solid electrolyte interphase (SEI) additive, was purchased from Solvay, dried, and distilled before use. All other reagents were purchased from either Sigma-Aldrich or Fisher Scientific.

Synthesis of Poly(acrylic acid-co-tetra(ethylene glycol) diacrylate) (branched PAA) by RAFT

Polymerization

To a 50-mL, two-necked round bottom flask equipped with a magnetic stir bar, the following were added: acrylic acid (AA, 6.630 g, 92.08 mmol), TEGDA (0.060 g, 0.20 mmol), 2-(2-cyanopropyl)dithiobenzoate (CPDB, 0.020 g, 0.09 mmol), 2,2'-azobis(2-methylpropionitrile) (AIBN, 0.004 g, 0.02 mmol), and dimethylformamide (DMF, 11.740 g). The mixture was degassed by three freeze-pump-thaw cycles, and then the flask was placed in an oil bath with a preset temperature of 70 °C. The polymerization progress was monitored by ¹H nuclear magnetic resonance (NMR) spectroscopy. After proceeding for 18 h, the polymerization was quenched by removing the flask from the oil bath and blowing the mixture with air flow. The mixture was diluted with 5 mL tetrahydrofuran (THF). Unreacted reagents were removed by precipitating the mixture in dichloromethane. The collected polymer was dissolved in THF. This dissolution/precipitation process was repeated three times. The polymer was then dried on a lyophilizer. By varying the feeding molar ratio between TEGDA and AA, three branched PAA samples were synthesized and were named **bPAA-1**, **bPAA-2**, and **bPAA-3**, with the corresponding feeding molar ratios [TEGDA]:[AA] as 0.05, 0.1, and 0.2, respectively. A linear PAA binder with comparable molecular weight was also synthesized by RAFT polymerization.

Physiochemical and Electrochemical Properties of Polymer Binders

The NMR spectrum (¹H) was recorded on a Bruker 300 NMR spectrometer at room temperature. The molecular weight of the branched PAA, as well as the linear PAA polymer binders, were characterized by gel permeation chromatography/size exclusion chromatography (GPC/SEC). Notice that all the PAA samples here are methylated to ensure solubility in THF. A 10-mg polymer sample was dissolved in 2 mL THF, followed by the addition of a solution of

trimethylsilyldiazomethane in diethyl ether until the solution became yellow and stopped bubbling. The rheological properties of the polymer binders were characterized on a TA Instrument model Discovery HR-3 rheometer operating in a cone-plate geometry with a cone diameter of 20 mm and an angle of 2° (truncation 52 μm) using 10 wt% polymer aqueous solution (25 °C) and also using a stress ramp. The glass transition temperatures (T_g) of the polymer binders were measured by temperature-modulated differential scanning calorimetry (on a PerkinElmer DSC 6000) using dried polymer samples from -80 to 200 °C with a heating and cooling speed of 10 °C min⁻¹.

The Li⁺ conductivity of each polymer binder film was studied by using electrochemical impedance spectroscopy (EIS). Specifically, each polymer film with a Gen 2 electrolyte was sandwiched between two stainless steel spacers in a 2032-type coin cell in an argon-filled glove box. Then the electrochemical impedance of the cells was tested in the frequency range from 1 MHz to 0.1 Hz on a Solartron 1400 CellTest[®] System (0.01 V). Li⁺ conductivity can be calculated using the Z' intercept at a high frequency range obtained from the Nyquist plot of the EIS spectrum.

Adhesion Test

Adhesion tests of the silicon-graphite (Si-Gr) composite electrodes were conducted on an Instron 3343 universal test machine. The laminated side of the electrodes (3 inch × 1 inch) were attached to 3M 600 Scotch tape (1 inch in width). The lamination was peeled off the copper current collector by pulling the Scotch tape at the angle of 180° at a constant displacement rate of 10 mm/s. The applied force was continuously measured, and the load/displacement plots were produced.

Cell Assembly and Electrochemical Characterization

Each electrode lamination was coated on a copper foil current collector with a doctor blade from a thoroughly mixed coating slurry containing 73 wt% Hitachi MagE graphite, 15 wt% Si nanoparticles, 2 wt% C45 carbon black, and 10 wt% branched or linear PAA binders. **The loading**

of active materials of those electrodes was controlled at $\sim 3 \text{ mg cm}^{-2}$. The electrode was dried and calendared before being punched into 1.6 cm^2 circular disks. Then the electrodes were further dried in a vacuum oven at $130 \text{ }^\circ\text{C}$ for 8 h and were assembled in 2032-type coin cells. For half-cell evaluation, the cells were configured with a lithium metal counter electrode, a microporous polypropylene separator (Celgard 2325), a silicon-graphite (Si-Gr) composite electrode, and a Gen 2 electrolyte containing 10 wt% FEC (30 μL). The cells were cycled on a Maccor battery cycler for 100 cycles at C/3 rate after three C/20 formation cycles. The cutoff voltage is between 0.01 V and 1.5 V. The EIS of the cells was measured after 100 cycles in the frequency range of from 1 MHz to 0.1 Hz on a Solartron 1400 CellTest® System by applying a 10-mV voltage to the cells. For the full-cells assembly, the Si-Gr composite negative electrodes were first subjected to three formation cycles at a C/20 rate using half-cell configuration. Then the preformed Si-Gr composite negative electrodes were harvested and reassembled into full cells with matched NCM 523 positive electrodes. The full-cell testing protocol consisted of three formation cycles at a nominal C/20 rate, a hybrid pulse power characterization (HPPC) test, 92 aging cycles at a C/3 rate, another HPPC test, and three final cycles at a C/20 rate, for a total of 100 cycles with the cell voltage between 3.0–4.2 V. The HPPC test was used to investigate the direct current (DC) resistance of full cells at different depths of discharge (DOD). A specific test procedure is as follows: cells were first charged at a C/3 rate until the voltage reached 4.2 V, and then were discharged at C/3 for 10% DOD, and rested at open circuit voltage (OCV) for 1 hour. After that, a discharge pulse at 3C for 10 sec, a rest for 40 sec, a charge pulse at 2.25C for 10 sec, and a rest for 60 sec. The resistance was calculated by using current and voltage differences before and after the HPPC discharge pulses.

Post-Cycling Analysis

The cycled cells were disassembled in an argon-purged glovebox, and the electrodes harvested were then rinsed with anhydrous dimethyl carbonate and dried in a vacuum oven. The morphologies of the pristine and cycled electrodes were examined using a JEOL JCM-6000Plus scanning electron microscope (SEM). Fourier-transform infrared (FTIR) spectra of these electrodes were obtained using a Thermo Scientific Nicolet iS5 spectrometer located in a glove box filled with Ar.

Results and Discussion

Introducing a cross-linking architecture to polymer binders is an effective approach to take to enhance mechanical properties so that the volume changes of silicon anodes upon lithiation can be better accommodated.^{20, 27-28} However, highly cross-linked polymer usually becomes insoluble, which makes it practically impossible to perform slurry processing. Our approach is not to directly cross-link the linear PAA backbones, but rather to co-polymerize the AA monomer with a controlled amount of ether chains via RAFT polymerization. This way, the resulted copolymers actually have a branching architecture. The branching architecture can be beneficial for polymer binders as it may promote mechanical strength while still maintain processability. **Figure 1a** illustrates the structures of the synthesized branched PAA polymers, in which PAA is branched by ether chains. This design features several advantages, as shown in **Figure 1b**: first, the dominating component is still PAA as we are controlling the ether content to a very small percentage; therefore, most merits of the PAA binder remain, such as its excellent adhesion to SiNPs via the bonding between carboxylic acid groups and silanol (Si-OH) groups on the surface of the SiNPs. Second, PEG chains may also promote Li ionic conductivity as mentioned previously, which is also a mostly desirable property for enhanced performance. Finally, the branching architecture is extremely useful for tuning mechanical properties that affect electrode integrity, which is crucial for accommodating the volume changes of SiNPs during cycling. RAFT polymerization is a type

of controlled polymerization involving a conventional radical polymerization mediated by chain transfer agent (CTA). Therefore, the molecular weight (M_w) and branching density of the polymers can be statistically controlled by adjusting the molar ratio between the acrylate acid monomer (AA) and CTA, as well as that between AA and the cross-linker.²⁹⁻³¹ We selected tetra(ethylene glycol) diacrylate (or TEGDA) as the branching agent given that its short ether chain may facilitate Li ionic conductivity while alleviating the crystallinity of the polymer chains.³² The feed ratio of TEGDA is carefully adjusted so that the synthesized bPAA binders are modified in a very mild way and remain soluble in water and processable in a lamination slurry. Three bPAA binders with different molar feed ratios from 0.05-0.2 were synthesized. Further increasing the feed ratio (0.5) leads to an insoluble polymer that is no longer suitable for binder application and is not further evaluated. It should be noted that the synthesized polymers are not soluble in the carbonate based electrolyte. As a representative example, **Figure 2** compares the NMR spectra of bPAA-3 and linear PAA. The newly appeared peak at 4.3 ppm shown in the spectra of bPAA-3 is assigned to the proton of $O=C-O-CH_2-$, confirming the formation of ester bonding between PAA and TEGDA. The characterization results of the three binders, including molecular weight, feed ratio, measured ratio, degree of polymerization (DP), and glassy temperature (T_g) are summarized in **Table 1**. The molecular weights of those three binders were made comparable (determined by GPC in **Figure S1a**) for comparison, and the actual ratio of [TEGDA]:[PAA] in the polymer can be obtained by calculating the ratio of the integration of NMR peaks of the ester protons ($O=C-O-CH_2-$) and the PAA backbone ($-CH_2-CH_2-$) (see **Figure S2** for details).³³ The measured ratio of TEGDA to PAA based on NMR peaks is larger than the feed ratio mainly due to the different reactivity of the two reagents. A retardation effect was found for AA monomer when it was copolymerized with acrylic ester, probably resulting from ionic repulsion of AA in the polar solvent like DMF, and thus

reduced effective monomer concentration.³⁴⁻³⁵ However, statistically, the trend of the measured ratio is consistent with the feeding ratio, and we have synthesized the polymers with reproducible measured ratios. A linear PAA binder with comparable DP was synthesized as a control sample.

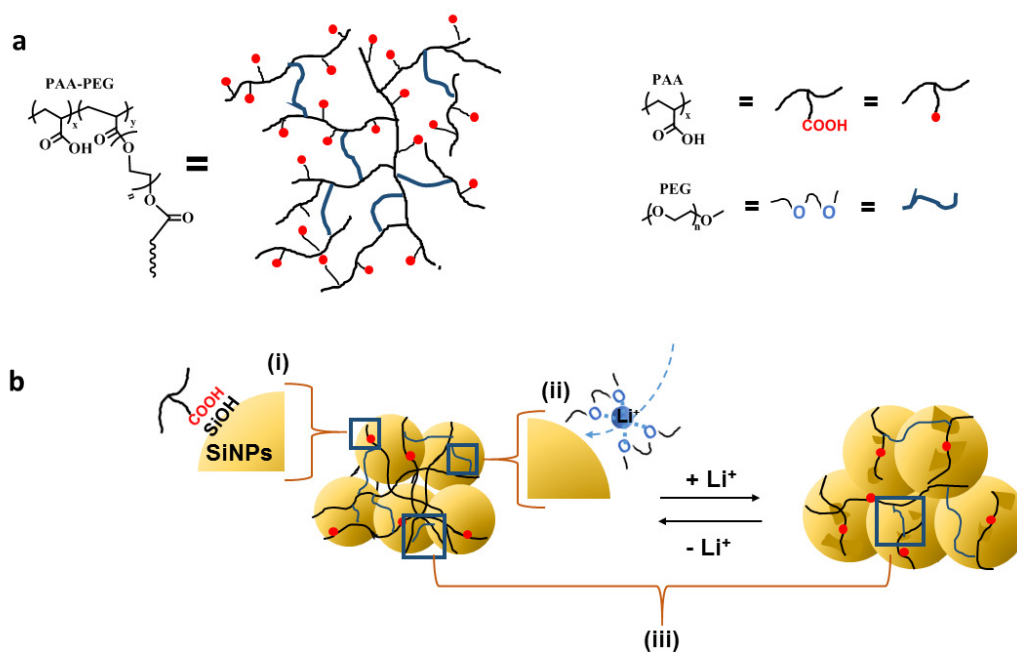


Figure 1. (a) Schematic structure of branched PAA binder. (b) Schematic illustration of the design strategy of the branched PAA binder: (i) adhesion between SiNPs promoted by interaction between the carboxylic acid of the PAA and the Si-OH group on the SiNP surface; (ii) Li⁺ conductivity facilitated by ether chains; and (iii) electrode integrity enhanced by the branched polymer chains.

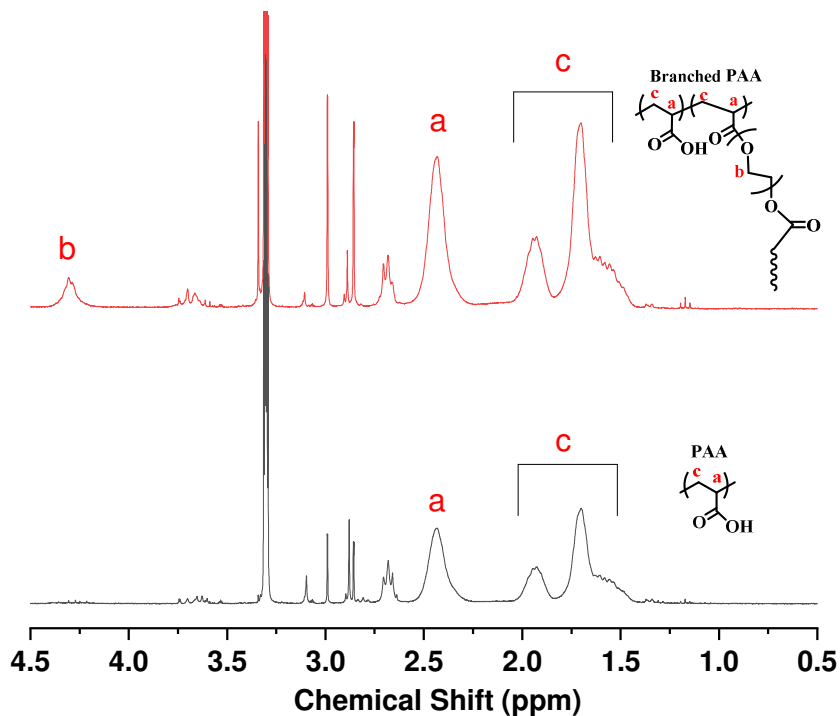


Figure 2. ^1H NMR spectrum bPAA-3 (top, red curve) and PAA (bottom, black curve).

Table 1. Summary of the characterization results of the synthesized polymer binders, including feed ratio, $[\text{TEGDA}]:[\text{PAA}]$ % from NMR, degree of polymerization (DP), molecular weight, and glass transition temperature (T_g).

Binder	Feed ratio ($[\text{TEGDA}]:[\text{AA}]$, mol/mol)	$[\text{TEGDA}]:[\text{PAA}]$ % from NMR	DP	$M_{n,\text{SEC}}$, kDa	T_g , $^{\circ}\text{C}$
PAA	0	Not applicable	890	55.7	109.0
bPAA-1	0.05	0.71	736	72.7	95.0
bPAA-2	0.1	0.80	631	64.8	90.7
bPAA-3	0.2	0.93	648	59.0	87.2

As shown in Table 1, the measured $[\text{TEGDA}]:[\text{PAA}]$ % confirms the changes introduced by the feed ratio. As the feed ratio increases, the measured value increases, as well. However, the measured ratios are quite different from the feed ratios, which probably result from the difference in reactivity ratio between AA and TEGDA in DMF.³⁶ Interestingly, while DPs are relatively comparable (especially for bPAA-2 and bPAA-3), the measured average molecular weight (M_n)

is decreasing as TEGDA increases. This phenomenon has been observed by others,³⁷ and can be explained by the changes of hydrodynamic volumes. GPC separates polymers by hydrodynamic volume, and branching leads to a contraction of the polymer chain in terms of the hydrodynamic volume, thus resulting in decreased molecular weight.³⁸

In addition, branching the PAA backbone also affects the mechanical properties. As shown in **Figure 3a**, as TEGDA increases, the glass transition temperature, or T_g , of the synthesized binders decreases, indicating the improved flexibility of the binders that is desirable for silicon anodes. The observed dependence of T_g on the incorporated ether chain is consistent with previous reports regarding blended PAA and poly ethylene glycol polymers.³⁹⁻⁴⁰ Rheology property, such as viscosity, is another important parameter that plays a major role in the slurry-making process.²⁵ In **Figure 3b**, the apparent viscosity of the binder solutions were measured over various shear rates. The synthesized binders deliver much higher viscosities compared to PAA, indicating that the incorporated TEGDA, as well as the branching architecture, really do help to promote viscosity. This result is consistent with the reported rheology study of branched polymers in which the viscosity can reflect the branching degree of the polymers.⁴¹⁻⁴² On the other hand, the viscosity does not linearly relate to the increase of TEGDA as **bPAA-3** affords lower viscosity at high shear rate.⁴³ As for **bPAA-1** and **bPAA-2**, a non-Newtonian behavior (viscosity does not change over shear rate) is observed at lower shear rate; and only when the shear rate is above 10^2 is a shear-thinning effect seen. **For bPAA-3, the shear-thinning effect is more pronounced throughout the measuring range, which may result from the higher branching degree as branched polymers are more susceptible to shear thinning.**⁴³ While the M_n of those binders may play a role,^{15, 44-45} the branching could also contribute to these changes.⁴³ The power-law model is used to compare the shear-thinning effect in each binder:

$$\eta = K(\dot{\gamma})^{n-1} \quad (\text{Eq. 1}),$$

where η is the apparent viscosity, $\dot{\gamma}$ is the shear rate, K is the consistency index, and n is the flow behavior index. For a fluid exhibiting a shear-thinning effect, n is smaller than 1, and the smaller n is, the stronger the shear-thinning effect. By fitting the apparent viscosity in the shear rate range 10^2 – 10^3 s^{-1} , we can obtain the n values that are compiled and presented in **Table S1**. The branched PAA binders generally afford smaller n values, implying an enhanced shear-thinning effect. The combination of high viscosity at low shear rate and a strong shear-thinning effect at high shear rate is highly desirable for improving the stability of the slurries and facilitating the lamination process.²⁵

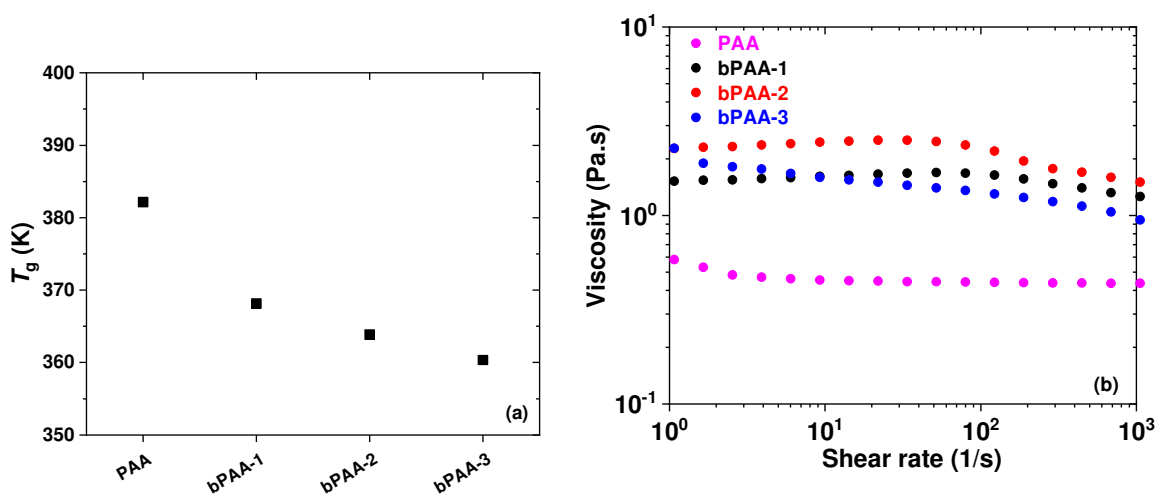


Figure 3. Mechanical properties of each polymer binder: (a) the plot of T_g (obtained from a temperature-modulated PerkinElmer DSC 6000) with respect to the ratio [TEGDA]:[PAA], and (b) apparent viscosity vs. shear rate at 25 °C.

The conductivity of the synthesized binders was characterized by electrochemical impedance spectroscopy. Thin films of the binders were made by laminating an aqueous solution of the binders on the Cu foil and drying them in the vacuum oven overnight. These films were then transferred into an argon-filled glovebox and were sufficiently wetted by a Gen 2 electrolyte before

they were sandwiched between two stainless steel spacers in a 2032-type coin cell. The assembled cell was then subjected to EIS measurement. Cell impedance was measured by applying a 10-mV perturbation in the frequency range of 100 kHz to 1 Hz at the OCV. The ohmic resistance (R), obtained from the Nyquist plot at the low-frequency end of the semicircle, was used to calculate the ionic conductivity using the following equation:

$$\sigma = \frac{1}{R} \times \frac{l}{A} \quad (\text{Eq. 2}),$$

where l is the thickness of the polymer film and A is the surface area of the film. As shown in Figure 4, the measured conductivity increases as the TEGDA increases, indicating that the incorporated ether moiety indeed facilitates the Li ionic conductivity, which is consistent with our speculation.

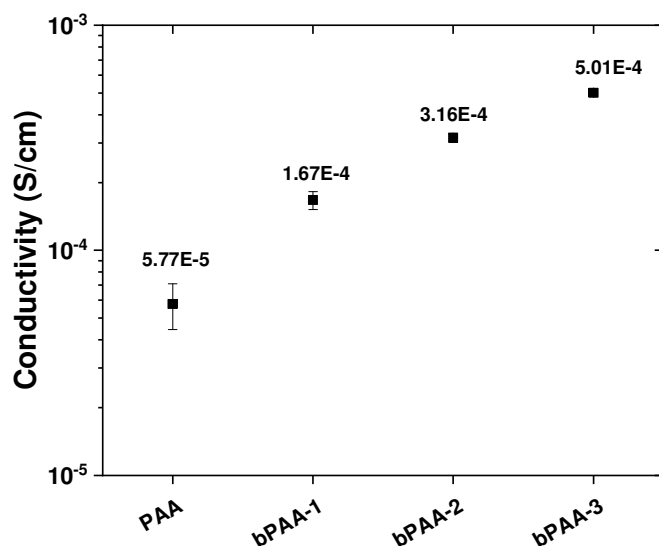


Figure 4. The Li ionic conductivity of each binder.

A peeling test was conducted on the Si-Gr electrode laminates fabricated using the synthesized binders in order to evaluate their adhesive/cohesive strength. Details regarding the test method can be found in the experimental section. As shown in **Figure 5**, the load/width values

reflect the binding strength of the binders used in the tested laminates. It is interesting to observe that with increased TEGDA, the binding strength is decreasing. Actually, this observation can also be attributed to the increased branching degree. In the electrode matrix, the binding strength results from the interaction between binder chains and active particles. Similar to GPC results that the decreased hydrodynamic volumes leads to decreased M_n ,³⁸ branched architecture of polymers can afford smaller effective length,⁴¹ which then adversely affects the binding strength as the shorter chains get less exposure to active particles.

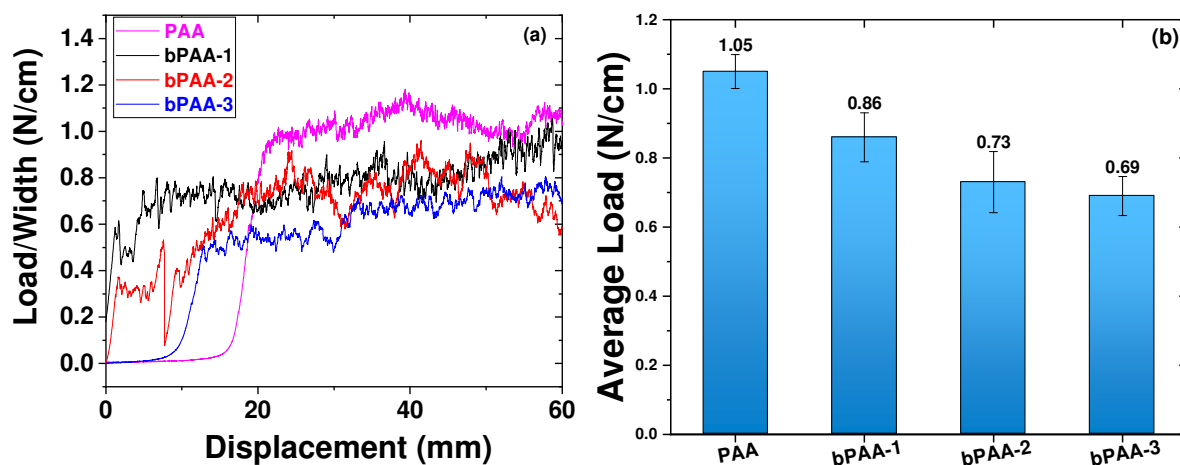


Figure 5. (a) The 180° peeling test results for the Si-Gr electrodes using bPAA and PAA binders, and (b) average load/width with a range of 50 mm for the corresponding electrodes.

While the new binders show some mixed property changes, the ultimate evaluation comes down to cell cycling performance. **Figure 6** and **Table 2** compile the electrochemical characterizations of half-cells using Si-Gr composite electrodes fabricated with various binders. The specific capacity was calculated based on the weight of active materials used in the anode, including graphite and silicon. It is encouraging to see that the electrodes with branched PAA binders show improved electrochemical performance. Specifically, except for the **bPAA-1** binder, the synthesized binders show improved initial capacity and capacity retention compared with those of linear PAA binder, and this improvement is more pronounced when TEGDA increases. For

instance, the best-performing **bPAA-3** cell affords 752 mAh/g of initial capacity and 76% capacity retention, which are significantly higher than those of the linear PAA cell (678 mAh/g and 45%).

The Coulombic efficiency (CE) also reflects the cyclability by showing capacity discrepancy of charging and discharging processes, and the results are consistent with the capacity profiles with bPAA-3 electrode exhibiting the highest CE while PAA electrode bearing the lowest.

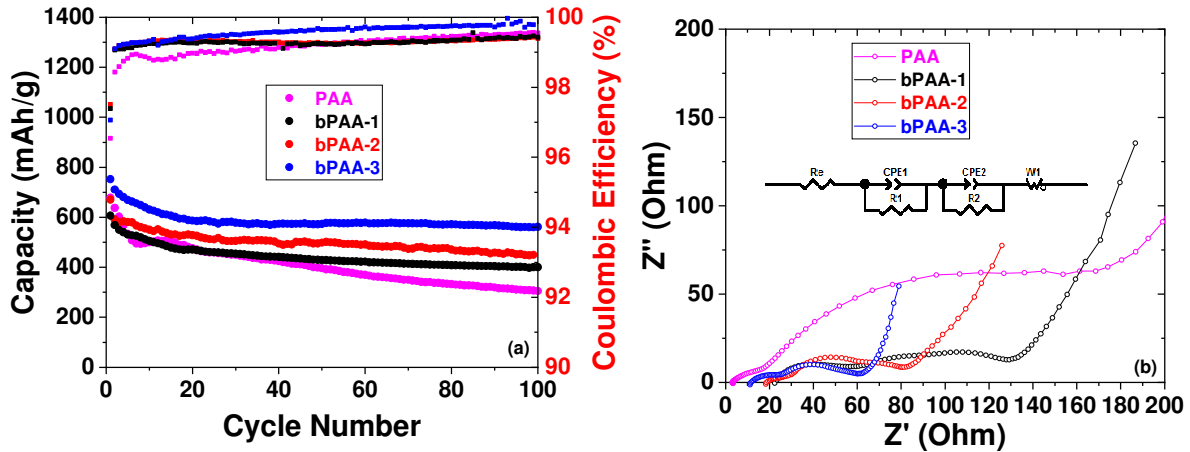


Figure 6. Electrochemical characterizations of half-cells containing Si-Gr electrodes fabricated using branched PAA binders: (a) specific delithiation capacity profiles (to the left) and Coulombic efficiency profiles (to the right); and (b) EIS measurements after 100 cycles (C/3).

Table 2. Loading density, initial specific capacity, initial Coulombic efficiency, capacity retention, and interfacial resistance results of cells assembled with lithium metal/Si-graphite electrodes using both branched and linear PAA binders.

Electrode	Loading, mg/cm ²	Initial capacity, mAh/g ^a	Initial Coulombic efficiency, % ^b	Capacity retention, % ^c	Interfacial resistance, Ω ^d
PAA	2.7	678	96.5	45	101.9 ± 5.5
bPAA-1	2.4	607	97.5	66	91.5 ± 6.0
bPAA-2	2.7	670	97.4	67	50.5 ± 2.7
bPAA-3	2.4	752	97.1	76	40.5 ± 3.6

^{a, b} Determined at the first cycle of the C/3 cycle.

^c After 100 cycles at C/3.

^d Combined (R1 + R2).

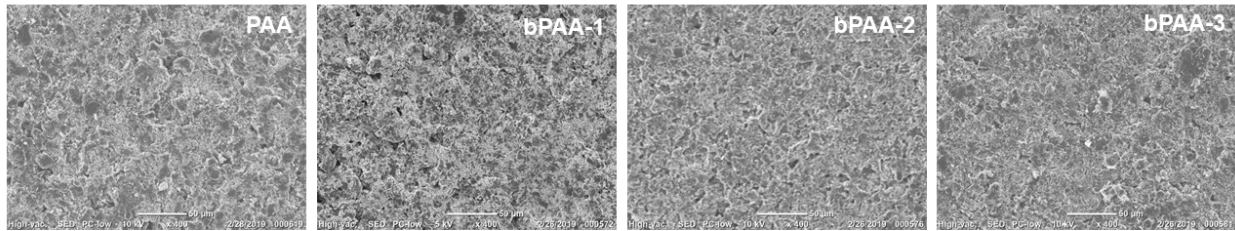
The observed high conductivity of the new binders in **Figure 4** is also reflected in cycling performance. EIS measurements were conducted on the half-cells after 100 cycles, and the results are shown in **Figure 6b**. Apparently, the increased TEGDA content prompts less resistance from the half-cell. From PAA to branched PAA cells, we observed a huge improvement in the impedance, judging by the reduction of the two semi circles of the impedance spectra. All of the Nyquist plots of the measured impedance spectra contain two semicircles from a high-frequency range to a middle-frequency range, which are generally referred to as the interfacial resistance caused by SEI buildup and the charge transfer interfacial resistance, respectively.⁴⁶ An equivalent circuit (shown as an inset in **Figure 6b**) is used to fit the plot, and the combined interfacial resistance (R_1 plus R_2) of each electrode is summarized in **Table 2**. Notice that in the equivalent circuit, R_e refers to the bulk resistance of the electrolyte and electrode, and W_0 is the Warburg impedance controlled by diffusion.⁴⁶⁻⁴⁹ According to the results, the interfacial resistance reduces as TEGDA content increases, which may be one major factor that contributes to the improved cycling performance. On the other hand, the adversely affected binding strength of the synthesized binders could result in more capacity fade due to delamination. Therefore, these two factors collectively lead to a somewhat mixed performance of the **bPAA-1** cell; but it is much improved performance when impedance dominates, such as in the **bPAA-2** and **bPAA-3** cells.

Surface characterization of the fabricated and cycled electrodes was performed using scanning electron microscopy (SEM). **Figure 7** summarizes the SEM images of the electrodes before and after cycling. Before cycling, all electrodes show good integrity of the laminates; but after 100 cycles, only **bPAA** electrodes still maintain much better integrity than the linear **PAA** electrode and with fewer cracks found on the surface. The cross-sectional images reveal that the increased TEGDA helps to reduce the volume expansion from 130% for the linear **PAA** electrode

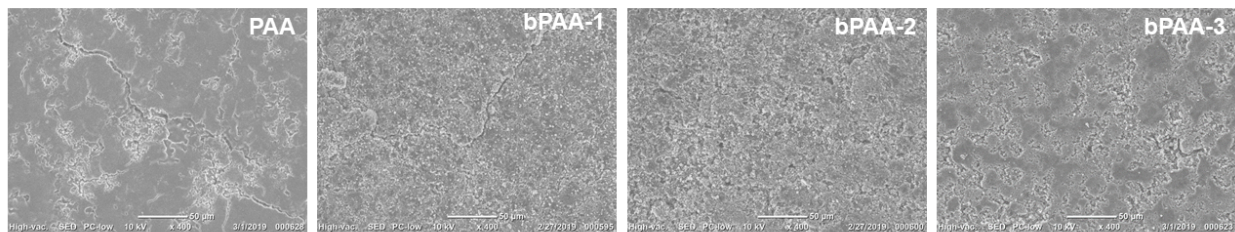
to 10% for the **bPAA-3** electrode. This dramatic improvement indicates that the branched PAA binders may be more suitable for accommodating the volume changes of Silicon particles, which may possibly be due to the enhanced flexibility evidenced by the lowered T_g . This observed enhancement of electrode matrix integrity is of crucial significance, as not only can the binders effectively hold the active particles together during cycling, but they can also prevent excessive SEI growth. These two factors may also contribute to impedance control.

(1)

Before Cycle

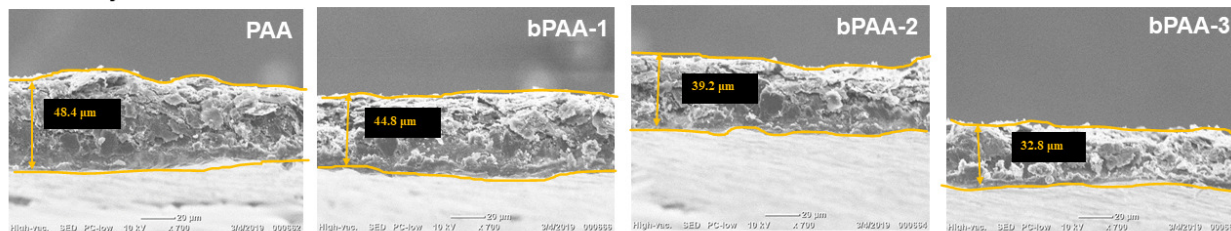


After Cycle



(2)

Before Cycle



After Cycle

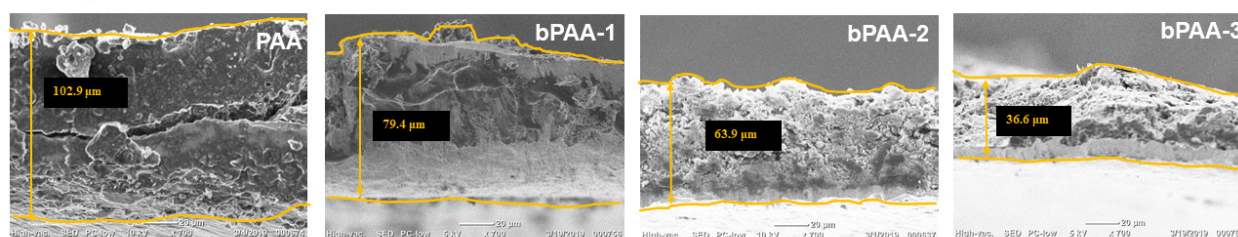


Figure 7. Morphology studies: (1) SEM images of Si-Gr electrodes from PAA and bPAA cells both before and after 100 cycles at the C/3 rate. The images are at 400 times magnification; and (2) cross-sectional SEM images of Si-Gr electrodes from PAA and bPAA cells both before and after 100 cycles at the C/3 rate. The images are at 700 times magnification.

FTIR is used to further analyze the composition of electrode surfaces (**Figure 8**). Before cycling, while the characteristic peaks of the $-\text{CO}_2\text{H}$ of PAA at 1685 cm^{-1} (C=O band) are observed for all electrodes, only bPAA electrodes show peaks at $2800\text{--}2900\text{ cm}^{-1}$ (C-H band), indicating the existence of ether chains. It is worth noting that the ether peaks remain nearly unchanged after 100 cycles, suggesting great stability even after prolonged exposure to the electrolyte. Also observed on the FTIR spectra of the cycled electrodes were a $-\text{COO}^-\text{Li}^+$ peak from the PAA binder (1562 and 1414 cm^{-1}) and from SEI formation (1308 cm^{-1} for $\text{Li}_2\text{C}_2\text{O}_4$ and 839 cm^{-1} for Li_2CO_3), which resulted from the repeated lithiation and delithiation processes. The intensity of these peaks is much lower for the linear PAA electrode, implying a less sturdy SEI layer.

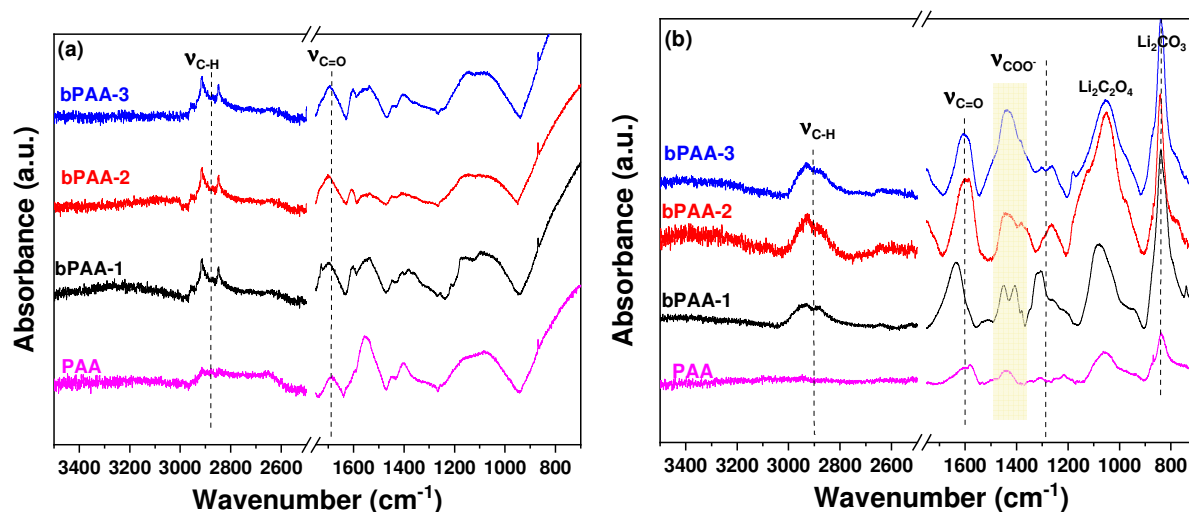


Figure 8. Fourier-transform infrared spectra of the Si-graphite electrodes showing each binder before (a) and after 100 cycles (b).

Finally, the best-performing binder is evaluated in full cells. The Si-Gr electrodes containing the PAA and **bPAA-3** binders are assembled against matched NCM 523 cathodes, and a standard cycling procedure is used for comparison (details can be found in the **Experimental Section**). **Figure 9** compiles the capacity and efficiency profiles, as well as the area specific impedance (ASI) results, and other parameters can be found in **Table S1**. As expected, the **bPAA-3** cell outperforms the PAA cell marginally in mostly all of the aspects, including initial capacity, average capacity, and capacity retention and ASI, indicating that we may have hit a “sweet spot” with the branched TEGDA-containing binders for balancing the properties that are desired for silicon electrodes.

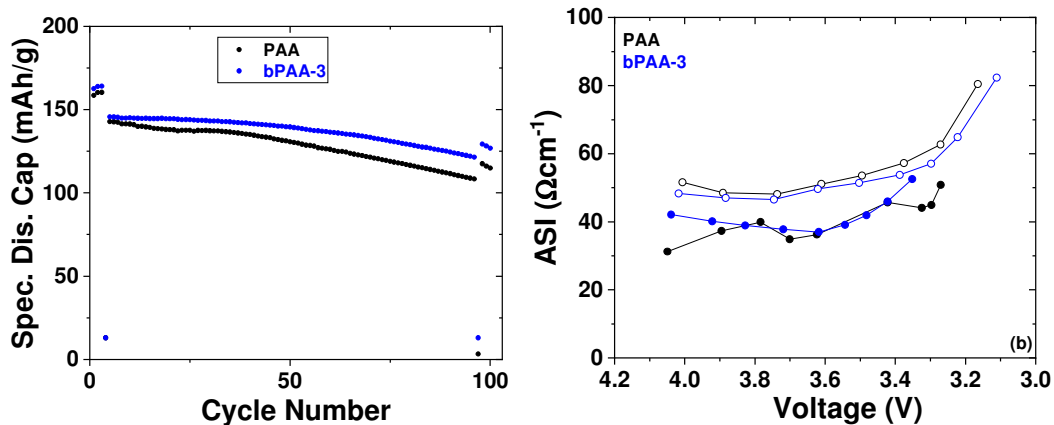


Figure 9. (a) Specific discharge capacity (to the left) and Coulombic efficiency (to the right) of cells assembled with the NCM 523 electrode/Si-Gr electrode using linear PAA (black) and **bPAA3** (blue) as binder (after 92 C/3 cycles after 3 C/20 cycles) and (b) area-specific impedance (ASI) vs. cell voltage before (solid circle) and after (empty circle) the C/3 cycles.

Conclusion

A series of novel branched polymeric binders were developed by copolymerizing acrylic acid (monomer) and ether chain containing TEGDA (as a cross-linker) using reversible addition-fragmentation chain transfer, or RAFT, polymerization. By carefully adjusting the feed ratio between the monomer and cross-linker, we are able to control the composition as well as the branching degree of the binders, which, in turn, show gradually tuned properties, such as improved viscosity of binder solutions, binding strength, glass transition temperature, and conductivity. While we do observe that the new binders show weakened binding strength, the introduced cross-linking ether **chains are** positively related with enhanced flexibility, shear-thinning effect at high shear rate, and ionic conductivity. This new set of combined properties turns out ultimately to effect the cycling performance of the corresponding Si-Gr electrodes in a very positive way. Half-cell evaluation shows that cycling performance improves as more TEGDA is introduced except for in the case of the **bPAA-1** cell; and the best-performing **bPAA-3** cell affords 752 mAh/g of initial capacity and 76% capacity retention, values that are significantly higher than those of the

PAA cell (at 678 mAh/g and 45%). In full cells, **bPAA-3** also exhibited well-rounded improvement over the PAA cells in terms of initial capacity, average capacity, capacity retention, and impedance, indicating great potential for practical applications in lithium-ion batteries. Surprisingly, the cross sectional SEM images indicate that the electrode expansion is much better controlled using **bPAA** binders as a drastic improvement from 110% to 10% expansion is observed. The results demonstrate when designing a polymeric binder, one should consider balancing different desired properties. This work exemplifies this approach by bringing in enhanced flexibility, conductivity and branching architecture of the binders, which synergistically lead to a well around binder materials with drastically reduced electrode expansion and improved cycling performance.

Acknowledgments

This research is supported by the U. S. Department of Energy, Vehicle Technologies Office (DOE-VTO). Argonne National Laboratory is operated for DOE Office of Science by UChicago Argonne, LLC, under contract number DE-AC02-06CH11357. Use of the Center for Nanoscale Materials, an Office of Science user facility, was supported by the U.S. Department of Energy, Office of Science, Office of Basic Energy Sciences, under Contract No. DE-AC02-06CH11357. We would like to thank the Cell Analysis, Modeling, and Prototyping (CAMP) facility of Argonne for providing the electrode materials. The authors declare no competing financial interests.

Supporting Information

GPC data of methylated binder; ¹H NMR spectrum of **bPAA-3**; Flow index (*n*) in Eq. 1 for each binder; N/P ratio, initial specific discharge capacity, initial Coulombic efficiency, average

capacity and capacity retention results of cells assembled with NCM523/Si-graphite electrodes using PAA and **bPAA-3** binder, respectively.

Keywords

Polymer binder, Silicon anode, Branched PAA, Lithium-ion batteries

References

1. Armand, M.; Tarascon, J. M., Building better batteries. *nature* **2008**, *451* (7179), 652-657.
2. Tarascon, J. M.; Armand, M., Issues and challenges facing rechargeable lithium batteries. *Nature* **2011**, 171-179.
3. Sun, Y.; Liu, N.; Cui, Y., Promises and challenges of nanomaterials for lithium-based rechargeable batteries. *Nat. Energy* **2016**, *1* (7), 16071.
4. Park, C.-M.; Kim, J.-H.; Kim, H.; Sohn, H.-J., Li-alloy based anode materials for Li secondary batteries. *Chem. Soc. Rev.* **2010**, *39* (8), 3115-3141.
5. Feng, K.; Li, M.; Liu, W.; Kashkooli, A. G.; Xiao, X.; Cai, M.; Chen, Z., Silicon - Based Anodes for Lithium - Ion Batteries: From Fundamentals to Practical Applications. *Small* **2018**, *14* (8), 1702737.
6. Wu, H.; Cui, Y., Designing nanostructured Si anodes for high energy lithium ion batteries. *Nano Today* **2012**, *7* (5), 414-429.
7. Chae, S.; Ko, M.; Kim, K.; Ahn, K.; Cho, J., Confronting Issues of the Practical Implementation of Si Anode in High-Energy Lithium-Ion Batteries. *Joule* **2017**, *1* (1), 47-60.

8. Chou, S.-L.; Pan, Y.; Wang, J.-Z.; Liu, H.-K.; Dou, S.-X., Small things make a big difference: binder effects on the performance of Li and Na batteries. *Phys. Chem. Chem. Phys.* **2014**, *16* (38), 20347-20359.
9. Nguyen, C. C.; Yoon, T.; Seo, D. M.; Guduru, P.; Lucht, B. L., Systematic Investigation of Binders for Silicon Anodes: Interactions of Binder with Silicon Particles and Electrolytes and Effects of Binders on Solid Electrolyte Interphase Formation. *ACS Appl. Mater. Interfaces* **2016**, *8* (19), 12211-12220.
10. Li, J.-T.; Wu, Z.-Y.; Lu, Y.-Q.; Zhou, Y.; Huang, Q.-S.; Huang, L.; Sun, S.-G., Water Soluble Binder, an Electrochemical Performance Booster for Electrode Materials with High Energy Density. *Adv. Energy Mater.* **2017**, *7* (24), 1701185.
11. Li, J.; Lewis, R. B.; Dahn, J. R., Sodium carboxymethyl cellulose a potential binder for Si negative electrodes for Li-ion batteries. *Electrochem. Solid-State Lett.* **2007**, *10* (2), A17-A20.
12. Magasinski, A.; Zdyrko, B.; Kovalenko, I.; Hertzberg, B.; Burtovyy, R.; Huebner, C. F.; Fuller, T. F.; Luzinov, I.; Yushin, G., Toward Efficient Binders for Li-Ion Battery Si-Based Anodes: Polyacrylic Acid. *ACS Applied Materials & Interfaces* **2010**, *2* (11), 3004-3010.
13. Kovalenko, I.; Zdyrko, B.; Magasinski, A.; Hertzberg, B.; Milicev, Z.; Burtovyy, R.; Luzinov, I.; Yushin, G., A Major Constituent of Brown Algae for Use in High-Capacity Li-Ion Batteries. *Science* **2011**, *334* (6052), 75-79.
14. Hu, B.; Jiang, S.; Shkrob, I. A.; Zhang, S.; Zhang, J.; Zhang, Z.; Zhang, L., Poly(4-vinylbenzoic acid): A Re-Engineered Binder for Improved Performance from Water-Free Slurry Processing for Silicon Graphite Composite Electrodes. *ACS Appl. Energy Mater.* **2019**.

15. Hu, B.; Shkrob, I. A.; Zhang, S.; Zhang, L.; Zhang, J.; Li, Y.; Liao, C.; Zhang, Z.; Lu, W.; Zhang, L., The existence of optimal molecular weight for poly(acrylic acid) binders in silicon/graphite composite anode for lithium-ion batteries. *J. Power Sources* **2018**, *378*, 671-676.
16. Jiang, S.; Hu, B.; Sahore, R.; Zhang, L.; Liu, H.; Zhang, L.; Lu, W.; Zhao, B.; Zhang, Z., Surface-Functionalized Silicon Nanoparticles as Anode Material for Lithium-Ion Battery. *ACS Appl. Mater. Interfaces* **2018**, *10* (51), 44924-44931.
17. Wu, H.; Yu, G.; Pan, L.; Liu, N.; McDowell, M. T.; Bao, Z.; Cui, Y., Stable Li-ion battery anodes by in-situ polymerization of conducting hydrogel to conformally coat silicon nanoparticles. *Nat. Commun.* **2013**, *4*, 1943.
18. Choi, S.; Kwon, T.-w.; Coskun, A.; Choi, J. W., Highly elastic binders integrating polyrotaxanes for silicon microparticle anodes in lithium ion batteries. *Science* **2017**, *357* (6348), 279-283.
19. Koo, B.; Kim, H.; Cho, Y.; Lee, K. T.; Choi, N. S.; Cho, J., A highly cross - linked polymeric binder for high - performance silicon negative electrodes in lithium ion batteries. *Angew. Chem. Int. Ed.* **2012**, *51* (35), 8762-8767.
20. Lim, S.; Chu, H.; Lee, K.; Yim, T.; Kim, Y.-J.; Mun, J.; Kim, T.-H., Physically Cross-linked Polymer Binder Induced by Reversible Acid–Base Interaction for High-Performance Silicon Composite Anodes. *ACS Appl. Mater. Interfaces* **2015**, *7* (42), 23545-23553.
21. Wei, L.; Hou, Z., High performance polymer binders inspired by chemical finishing of textiles for silicon anodes in lithium ion batteries. *J. Mater. Chem. A* **2017**, *5* (42), 22156-22162.
22. Lopez, J.; Chen, Z.; Wang, C.; Andrews, S. C.; Cui, Y.; Bao, Z., The effects of cross-linking in a supramolecular binder on cycle life in silicon microparticle anodes. *ACS Appl. Mater. Interfaces* **2016**, *8* (3), 2318-2324.

23. Tsao, Y.; Chen, Z.; Rondeau-Gagne, S.; Zhang, Q.; Yao, H.; Chen, S.; Zhou, G.; Zu, C.; Cui, Y.; Bao, Z., Enhanced cycling stability of sulfur electrodes through effective binding of pyridine-functionalized polymer. *ACS Energy Lett* **2017**, *2* (10), 2454-2462.
24. Munaoka, T.; Yan, X.; Lopez, J.; To, J. W. F.; Park, J.; Tok, J. B. H.; Cui, Y.; Bao, Z., Ionically Conductive Self - Healing Binder for Low Cost Si Microparticles Anodes in Li - Ion Batteries. *Adv. Energy Mater.* **2018**, *8* (14), 1703138.
25. Hu, B.; Jiang, S.; Shkrob, I. A.; Zhang, J.; Trask, S. E.; Polzin, B. J.; Jansen, A.; Chen, W.; Liao, C.; Zhang, Z.; Zhang, L., Understanding of pre-lithiation of poly(acrylic acid) binder: Striking the balances between the cycling performance and slurry stability for silicon-graphite composite electrodes in Li-ion batteries. *J. Power Sources* **2019**, *416*, 125-131.
26. Xue, Z.; He, D.; Xie, X., Poly (ethylene oxide)-based electrolytes for lithium-ion batteries. *J. Mater. Chem. A* **2015**, *3* (38), 19218-19253.
27. Koo, B.; Kim, H.; Cho, Y.; Tae Lee, K.; Choi, N.-S.; Cho, J., A Highly Cross-Linked Polymeric Binder for High-Performance Silicon Negative Electrodes in Lithium Ion Batteries. *Angew. Chem. Int. Ed. Engl.* **2012**, *51*, 8762-8767.
28. Lim, S.; Lee, K.; Shin, I.; Tron, A.; Mun, J.; Yim, T.; Kim, T.-H., Physically cross-linked polymer binder based on poly(acrylic acid) and ion-conducting poly(ethylene glycol-co-benzimidazole) for silicon anodes. *J. Power Sources* **2017**, *360*, 585-592.
29. Chiefari, J.; Chong, Y. K.; Ercole, F.; Krstina, J.; Jeffery, J.; Le, T. P. T.; Mayadunne, R. T. A.; Meijs, G. F.; Moad, C. L.; Moad, G., Living free-radical polymerization by reversible addition– fragmentation chain transfer: the RAFT process. *Macromolecules* **1998**, *31* (16), 5559-5562.

30. Chong, Y. K.; Le, T. P. T.; Moad, G.; Rizzardo, E.; Thang, S. H., A more versatile route to block copolymers and other polymers of complex architecture by living radical polymerization: the RAFT process. *Macromolecules* **1999**, *32* (6), 2071-2074.
31. Moad, G.; Rizzardo, E.; Thang, S. H., Living radical polymerization by the RAFT process. *Aust. J. Chem.* **2005**, *58* (6), 379-410.
32. Fu, G.; Kyu, T., Effect of Side-Chain Branching on Enhancement of Ionic Conductivity and Capacity Retention of a Solid Copolymer Electrolyte Membrane. *Langmuir* **2017**, *33* (49), 13973-13981.
33. Speřvácěk, J. í.; Suchopárek, M.; Al-Alawi, S., Characterization of the stereochemical structure of poly(acrylic acid) by one- and two-dimensional ^{13}C - ^1H nuclear magnetic resonance spectra. *Polymer* **1995**, *36* (21), 4125-4130.
34. Paxton, T. R., Copolymerization reactivity ratios acrylic and methacrylic acids with butyl acrylate and butyl methacrylate. **1963**, *1* (2), 73-76.
35. Eldridge, R. J.; Treloar, F. E., Reactivity ratios for acrylic acid–methyl acrylate copolymerization in 1,4-dioxane. **1976**, *14* (11), 2831-2834.
36. Rudin, A.; Choi, P., Chapter 9 - Copolymerization. In *The Elements of Polymer Science & Engineering (Third Edition)*, Rudin, A.; Choi, P., Eds. Academic Press: Boston, 2013; pp 391-425.
37. Mori, H.; Seng, D. C.; Lechner, H.; Zhang, M.; Müller, A. H. E., Synthesis and Characterization of Branched Polyelectrolytes. 1. Preparation of Hyperbranched Poly(acrylic acid) via Self-Condensing Atom Transfer Radical Copolymerization. *Macromolecules* **2002**, *35* (25), 9270-9281.

38. Gaborieau, M.; Castignolles, P., Size-exclusion chromatography (SEC) of branched polymers and polysaccharides. *Anal Bioanal Chem* **2011**, 399 (4), 1413-1423.
39. Lu, X.; Weiss, R. A., Phase behavior of blends of poly (ethylene glycol) and partially neutralized poly (acrylic acid). *Macromolecules* **1995**, 28 (9), 3022-3029.
40. Bicerano, J.; Sammler, R. L.; Carriere, C. J.; Seitz, J. T., Correlation between glass transition temperature and chain structure for randomly crosslinked high polymers. *J. Polym. Sci., Part B: Polym. Phys.* **1996**, 34 (13), 2247-2259.
41. Fetters, L. J.; Kiss, A. D.; Pearson, D. S.; Quack, G. F.; Vitus, F. J., Rheological behavior of star-shaped polymers. *Macromolecules* **1993**, 26 (4), 647-654.
42. Wood-Adams, P. M.; Dealy, J. M., Using Rheological Data To Determine the Branching Level in Metallocene Polyethylenes. *Macromolecules* **2000**, 33 (20), 7481-7488.
43. Jabbarzadeh, A.; Atkinson, J. D.; Tanner, R. I., Effect of Molecular Shape on Rheological Properties in Molecular Dynamics Simulation of Star, H, Comb, and Linear Polymer Melts. *Macromolecules* **2003**, 36 (13), 5020-5031.
44. Senff, H.; Richtering, W., Influence of cross-link density on rheological properties of temperature-sensitive microgel suspensions. *Colloid. Polym. Sci.* **2000**, 278 (9), 830-840.
45. Yamaguchi, M., Rheological properties of linear and crosslinked polymer blends: Relation between crosslink density and enhancement of elongational viscosity. *J. Polym. Sci., Part B: Polym. Phys.* **2001**, 39 (2), 228-235.
46. Kwon, Y. H.; Minnici, K.; Huie, M. M.; Takeuchi, K. J.; Takeuchi, E. S.; Marschilok, A. C.; Reichmanis, E., Electron/Ion Transport Enhancer in High Capacity Li-Ion Battery Anodes. *Chem. Mater.* **2016**, 28 (18), 6689-6697.

47. Tang, K.; Fu, L.; White, R. J.; Yu, L.; Titirici, M.-M.; Antonietti, M.; Maier, J., Hollow Carbon Nanospheres with Superior Rate Capability for Sodium-Based Batteries. *Adv. Energy Mater.* **2012**, *2* (7), 873-877.
48. Su, M.; Wang, Z.; Guo, H.; Li, X.; Huang, S.; Xiao, W.; Gan, L., Enhancement of the Cyclability of a Si/Graphite@Graphene composite as anode for Lithium-ion batteries. *Electrochim. Acta* **2014**, *116*, 230-236.
49. Shobukawa, H.; Alvarado, J.; Yang, Y.; Meng, Y. S., Electrochemical performance and interfacial investigation on Si composite anode for lithium ion batteries in full cell. *J. Power Sources* **2017**, *359*, 173-181.